Glycoscience & Therapy 2 (2026) 100019

Contents lists available at ScienceDirect

Glycoscience & Therapy

journal homepage: www.keaipublishing.com/en/journals/glycoscience-therapy/

A recombinant lipidated receptor-binding domain is a promising self-adjuvanting antigen for mucosal vaccine

Huifang Xu[a,b,1], Tiantian Wang[a,1], Yanru Zhang[a,c], Han Wang[a], Shujuan Yu[a], Xuchen Hou[a], Bin Zhang[a], Peng Sun[a,d], Jun Wu[a,*], Bo Liu[a,*]

[a] Academy of Military Medical Sciences, Beijing 100071, China
[b] Department of Microbiology, School of Preclinical Medicine, Air Force Medical University, Shaanxi 710032, China
[c] College of Animal Science and Technology, College of Veterinary Medicine, Zhejiang Agriculture and Forestry University, Zhejiang 311300, China
[d] School of Basic Medical Sciences, Tsinghua University, Beijing 100084, China

ARTICLE INFO

Keywords:
Bacterial lipidation
SARS-CoV-2 RBD
Epitope-focused immunity
Mucosal nanovaccine

ABSTRACT

The SARS-CoV-2 pandemic has resulted in millions of fatalities, and the continual emergence of variants highlights the vital need for effective mucosal vaccines. Novel antigen designs and delivery strategies can elicit robust, epitope-focused mucosal immune responses while minimizing side effects and avoiding immune imprinting are urgently needed. Here, we developed an innovative bacterial lipidation-based SARS-CoV-2 receptor-binding domain (RBD) mucosal nanovaccine using the SpyCatcher/SpyTag (SC/ST) orthogonal assembly system. The lipidated SpyCatcher (lipoSC), derived from *Escherichia coli*, was employed as a nano-scaffold to display the SARS-CoV-2 RBD glycoprotein on its surface. The lipoSC-RBDST exhibited favorable monodispersity and thermostability, effectively promoted T follicular helper (Tfh) cell and germinal center B cell proliferation in endobronchial lymph nodes following mucosal administration, and was well tolerated overall. A series of animal experiments showed the potent ability of lipoSC-RBDST to activate RBD-specific mucosal immunity in the respiratory tract, as evidenced by the presence of neutralizing antibodies (nAbs) and secretory IgA (sIgA) in bronchoalveolar lavage fluid (BALF) and nasal lavage fluid (NLF). Serum neutralizing antibody titers remained above 10^3 even eight months post-immunization. There was also a significant increase in lung-localized tissue-resident memory (T_{RM}) T cells. Furthermore, two doses of mucosal booster activated and retained the omicron-specific immune responses in the respiratory track in wild-type RBD-primed mice. In conclusion, these findings support the utilization of a bacterial lipidation-based antigen design as a promising strategy for mucosal delivery to elicit epitope-focused mucosal immunity against SARS-CoV-2.

1. Introduction

The SARS-CoV-2 pandemic and the continual emergence of SARS-CoV-2 variants caused millions of fatalities.[1,2] Although vaccination has been a successful strategy for preventing and controlling the spread of this virus,[3] the majority of the approved vaccines against SARS-CoV-2, including inactivated vaccines,[4,5] mRNA vaccines,[6] viral-vectored vaccines,[7,8] and protein subunit vaccines,[9,10] are administered by intramuscular injections that induce systemic immunity and do not provide a first line of protection in the respiratory tract, as the response is deficient in secretory IgA (sIgA) and tissue-resident memory T (T_{RM}) cells.[11]

Mucosal vaccines, which induce both localized mucosal and systemic immunity characterized by sIgA, T_{RM} cells across the respiratory tract, and circulating antibodies,[12–14] have promise for eliminating infections and preventing the transmission of respiratory pathogens. Several mucosal vaccine candidates against SARS-CoV-2 are under development or have been authorized,[15] most of which are based on adenovirus or influenza virus or parainfluenza virus vectors.[15] Additionally, proteinaceous antigens, which are encapsulated with

* Corresponding authors.
E-mail addresses: xuhuifang9169@163.com (H. Xu), con_an@126.com (T. Wang), zhangyrnest@163.com (Y. Zhang), wanghan010811@163.com (H. Wang), shujuanyu24@126.com (S. Yu), hoxuch@163.com (X. Hou), zhangbin@bmi.ac.cn (B. Zhang), sunpeng990718@163.com (P. Sun), junwu1969@163.com (J. Wu), liubo7095173@163.com (B. Liu).
[1] These authors contributed equally to this study.

https://doi.org/10.1016/j.glycos.2025.100019
Received 7 September 2025; Received in revised form 9 December 2025; Accepted 12 December 2025
Available online 13 December 2025

liposome or organic polymers [16] and displayed on the surface of a nanocarrier with ligand-receptor specific interactions,[17] or an unadjuvanted spike protein,[18] have also displayed attractive efficacy. However, previous research has demonstrated that immune imprinting against conserved regions of a spike protein [19–21] or viral vectors [22,23] exhibits impaired vaccine efficacy.

Protein N-terminal lipidation in bacteria, initiated by a unique N-terminal signal peptide that contains a conserved lipobox motif (e.g., [LVI][ASTVI][GAS]C) and a cysteine residue vital for modification, which results in diacylation of the thiol group of the N-terminal cysteine and acylation of the and α-amino group, can interact with toll-like receptors 2 or 6 (TLR2/6) (diacylated lipoproteins) or TLR2/1 (triacylated lipoproteins) heterodimeric complexes, thereby activating the TLR2 signaling pathway to exert adjuvant effects.[24,25] Commercialized *Neisseria meningitidis* serogroup B vaccine Trumenba® demonstrated that the lipidated antigen, rLP2086, can consistently elicit one order higher of bactericidal activity titers than the nonlipidated forms.[26] Theoretically, lipoproteins contain highly hydrophobic diacylated or triacylated lipids at the N-terminus of the protein, as well as a high charge density on the surface of the folded polypeptide domains, which are highly amphiphilic. Purified lipoproteins, which are free of membrane components, are energetically favorable, such that the lipids of multiple molecules can associate with each other and form a hydrophobic core of a micelle, with the hydrophilic polypeptide domains on the outer layer assembled in a side-by-side manner, which is suitable antigen carrier for mucosal delivery.

Here, we present the development and evaluation of an innovative bacterial lipidation-based SARS-CoV-2 mucosal nanovaccine. The lipidated SpyCatcher (lipoSC) was synthesized in *Escherichia coli* and assembled into particles, with the capacity to form isopeptide bonds with SpyTag-labeled molecules. The SARS-CoV-2 receptor-binding domain (RBD) glycoprotein was generated in glycoengineered *Pichia pastoris* and conjugated with lipoSC, resulting in the lipoSC-RBDST nanoparticle. A series of experiments demonstrated the RBD-specific mucosal and systemic immune response activation potential of lipoSC-RBDST, as well as the rapid boost of cross-protection capabilities against SARS-CoV-2 variants. Our findings regarding bacterial lipidation-based viral glycoprotein mucosal nanovaccines provide essential functional insights that should be considered when developing epitope-focused mucosal vaccines against SARS-CoV-2 variants and other respiratory viruses.

2. Methods

2.1. lipoSpyCatcher (lipoSC) design and production

The *E. coli* murein lipoprotein signal peptide (GenBank, Cat. #: EU900370.1, MKATKLVLGAVILGSTLLAGC) was fused to the N-terminus of the SpyCatcher sequence utilizing the pelB signal peptide as a control, and a His-tag was added for purification. Both constructs were cloned into the pET30a vector between the *Nde*I and *Not*I restriction sites, and the plasmids were transformed into *E. coli* C43(DE3) competent cells (Sigma, Cat. #: CMC0019) via heat shock. Single colonies were inoculated into Luria-Bertani medium (0.5 % yeast extract, 1 % tryptone, 1 % NaCl, 1 μg/mL kanamycin) and grown until the optical density at 600 nm was 0.6. Then the cells were induced with 0.5 mM isopropyl β-D-1-thiogalactopyranoside (IPTG) for 12 h. After induction, bacterial cultures were centrifuged at 8500 rpm for 15 min, and the supernatant was discarded. The pellets were then resuspended in water, sonicated, and both the supernatant and precipitate were analyzed using 12 % SDS-PAGE and western blot to screen for positive clones. For large-scale production, cells were resuspended in Ni-A buffer (20 mM Tris-HCl, pH 7.5, 0.3 M NaCl, 5 mM imidazole, 1 % Triton X100) at 1:20 (w/v), sonicated, and centrifuged. The supernatant was purified employing Ni Sepharose 6 Fast Flow resin (Cytiva, Cat. #: 17531802). After loading, the target protein was eluted using a gradient of 10 %, 30 %, and 100 % Ni-B buffer (20 mM Tris-HCl, pH 7.5, 0.3 M NaCl, 500 mM imidazole, 1 % Triton X-100). The fractions containing the target protein were desalted and further purified using a Source 30Q column (Cytiva, Cat. #: 17127503), equilibrated with 10 column volumes of 30Q-A1 buffer followed by 10 column volumes of 30Q-A2 buffer (20 mM Tris-HCl, pH 7.5, 0.1 % Tween 80). The protein was then linearly eluted with a 0–50 % gradient of 30Q-B buffer (20 mM Tris-HCl, pH 7.5, 1 M NaCl, 0.1 % Tween 80), and then the eluted fractions were collected. The resulting protein was further separated using a Superdex™ 200 Increase 10/300 GL column (Cytiva, Cat. #: 28990946) with phosphate-buffered saline (PBS) as the buffer.

2.2. Design, preparation, and structural characterization of the RBDST protein

RBDST protein was expressed and purified as previously described.[27] Briefly, a SpyTag sequence was added to the C-terminus based on the amino acid sequence from position 319–534 of the spike (S) protein of the SARS-CoV-2 Delta variant (GenBank accession number OK091006.1). It was then inserted into the pPICZαA vector between the *Xho*I and *Not*I sites, generating the plasmid pPICZαA-RBDST. pPICZαA-RBDST was then linearized with *Bgl*II and transformed into glycoengineered *P. pastoris*.[27] Expression of the target protein was induced by methanol, and positive clones were identified by screening with 12 % SDS-PAGE. After the shake-flask culture was completed, the product was centrifuged at 8500 × g for 15 min. The harvested supernatant was purified as described previously.[27] The purified recombinant RBDST was assessed by SDS-PAGE, and then it was digested with peptide-N-asparagine amidase (PNGase) F at 37°C.

2.3. Design and purification of the SpyTag-XEC RBD

The SpyTag sequence was added to the N-terminus of the XEC variant RBD sequence (GenBank accession number XQC65592.1) and cloned into the *BamH*I and *Xho*I sites of the PCDNA3.1vector. A His-tag was also incorporated into the protein to facilitate purification. The resulting construct, PCDN13.1-STXEC, was transfected into Expi 293 F cells (Thermo Fisher Scientific, A14527CN) using ExpiFectamine 293 transfection reagent (Gibco, A14524), according to the manufacturer's instructions. Seventy-two hours post-transfection, the supernatant was collected by centrifugation at 8500 × g for 15 min and then the recombinant protein was purified. Initially, the sample was purified using an SP Fast Flow column (Cytiva, 17072910). After loading, the column was equilibrated with SP-A buffer (20 mM PB 6.5) and eluted with SP-B buffer (20 mM PB 6.5, 1 M NaCl) using a gradient of 10 %, 30 %, and 100 %. The samples containing the target protein were further purified by diluting the samples twofold with Ni-A buffer (20 mM Tris-HCl, pH 7.5, 0.5 M NaCl, 5 mM imidazole). The samples were then loaded onto a Ni Sepharose 6 Fast Flow column. The protein was eluted with a gradient of Ni-B buffer (20 mM Tris-HCl, pH 7.5, 0.5 M NaCl, 0.5 M imidazole) and collected for further use.

2.4. lipoSC-RBDST and SC-RBDST complex production

The prepared RBDST was incubated overnight at 4°C with lipoSC and SC at a molar ratio of 5:1 to form lipoSC-RBDST and SC-RBDST complexes, respectively. Due to the presence of unreacted RBDST remaining in the reaction, lipoSC-RBDST and SC-RBDST were purified utilizing a Superdex™ 200 Increase 10/300 GL column and a Superdex™ 75 Increase 10/300 GL (Cytiva, 29148723) column, respectively, with PBS as the mobile phase.

2.5. Purity analysis

The purity of the target proteins was assessed by size-exclusion chromatography high-performance liquid chromatography (SEC-

HPLC). Absorbance values at 214 nm were recorded. SEC-HPLC (TSK gel G2000SWXL, 5 μm, Φ7.8 × 300 mm) was performed using a mobile phase of 20 mM PB 7.0 containing 150 mM NaCl t a flow rate of 0.5 mL/min.

2.6. Dynamic light scattering (DLS)

The protein sample was diluted to a concentration of 100 μg/mL, and then 1 mL was placed into the sample chamber. Particle size distribution was measured using a Malvern particle size analyzer. Each sample was analyzed five times.

2.7. Transmission electron microscopy (TEM)

Samples were prepared by carefully placing a copper grid on a glass slide. Afterward, 10 μL of the sample was pipetted onto the copper grid and left to sit for 10 min, after which the excess liquid was gently removed with a small piece of filter paper. For staining, 10 μL of 3 % uranyl acetate was applied to the samples on the copper grid and allowed to sit for 1–3 min before the excess stain was removed using a small piece of filter paper. The copper grid was air-dried for 10 min before imaging with TEM (JEOL Ltd., Japan) at an acceleration voltage of 100 kV.

2.8. Stability analysis of lipoSC-RBDST

The temperature stability of lipoSC-RBDST was analyzed by storing it at –20°C, 4°C, 25°C and 37°C for seven days with daily particle size measurements employing DLS.

2.9. Mass spectrometry analysis

Mass spectrometry analysis of lipoSC was carried out using a high-resolution mass spectrometer (TripleTOF 5600, AB Sciex) coupled with an ultra-high-performance liquid chromatography system (Waters Acquity UPLC). Data deconvolution was performed utilizing IntactMass software (Protein Metrics). The liquid chromatography separation was performed using a C4 column (5 μm, 2.1 × 150 mm, Symmetry300, Waters), with a mobile phase consisting of 0.1 % formic acid in water (A) and 0.1 % formic acid in acetonitrile (B). Mass spectrometry was conducted in positive ion mode with ion source parameters set as GS1 = 50, GS2 = 50, CUR = 30, TEM = 500, and ISVE = 5500. The compound parameters were DP = −80 and CE = −10, with a parent ion scan range of *m/z* 600–4000.

2.10. Luciferase reporter gene assay for NFκB activation

293T-NFκB-Luc cells (Zhejiang Meisen Cell Technology, Cat. #: CTCC-DZ-0179) were seeded in a 10-cm plastic dish at a density of 5×10^5 cells/well (Corning, Cat. #: 430167) and incubated for 12 h at 37°C with 5 % CO_2. The cells were transfected with 7.5 μg of PCDN13.1-TLR2 (synthesized by Sangon Biotech (Shanghai)) and 7.5 μg of pRL-TK plasmid (preserved by our laboratory) as an internal control using lipofectamine transfection reagent (Invitrogen, Cat. #: L3000015) for 6 h. The transfection medium was then replaced with complete DMEM medium, and the cells were maintained for 24 h. The transfected cells were replaced into a 6-well plate (Corning, Cat. #: 3516) and stimulated with equimolar amounts of Pam3CSK4 (InvivoGen, Cat. #: tlrl-pms), lipoSC, or SC for 1, 3, and 6 h. The cells were treated with lysis reagent, and the luciferase activity was determined using a dual luciferase assay kit (Vazyme, Cat. #: DL101). The luciferase activity in the cell lysates was determined with a microplate reader (SpectraMax® iD3), and the increase was expressed using the ratio in comparison to control cells.

2.11. Real-time quantitative polymerase chain reaction (RT-qPCR)

DC 2.4 cells were seeded in 6-well plates at a density of 5×10^5 cells/mL per well. The cells were incubated for 12 h at 37°C with 5 % CO_2 and then stimulated with equimolar amounts of Pam3CSK4, lipoSC, or SC for 6 h. RNA was isolated using the TRIzol® reagent (Invitrogen, Cat. #: 15596026) following the manufacturer's instructions. The purity of the extracted RNA was determined using a NanoDrop spectrophotometer (Thermo Fisher Scientific) by assessing the optical density ratio (OD260/280). The RNA was then reverse-transcribed into complementary DNA (cDNA) using a reverse transcription kit (Accurate Biotechnology, Cat. #: AG11728) following the provided protocol. qPCR was utilized to quantify the expression levels of the target genes using the synthesized cDNA as templates. The sequences of the primers (5′→3′) used in this study are listed in Table S1. qPCR reactions were carried out in a 20 μL system consisting of 1 μL of cDNA, 0.8 μL of primers, 10 μL of 2 × Hieff® qPCR SYBR Green Master Mix (Yeasen Biotechnology, Cat. #: 11201ES03), and 8.2 μL of DEPC-treated water (Thermo Fisher Scientific, Cat. #: AM9906). The PCR program used was as follows: an initial denaturation at 95°C for 3 min, followed by 39 cycles of 95°C for 10 s, 55°C for 20 s (annealing), and 72°C for 20 s (extension). The relative mRNA expression levels of TLR2 were normalized to those of β-actin using the $2^{-\Delta\Delta Ct}$ method.

2.12. Antigen phagocytosis by macrophages

LipoSC and SC were conjugated with the SpyTag-enhanced green fluorescent protein (ST-EGFP) in vitro at 4°C for 12 h. Following the incubation, the conjugates (20 μg/mL) were incubated with macrophages (provided by Yu Shujuan) for 24 h. Fifteen minutes prior to the end of the incubation, Hoechst stain (Thermo Fisher Scientific, Cat. #: H21486) was added to each well (10 μL/well) for nuclear staining. The staining solution was then discarded, and the cells were washed twice with PBS. Cells were fixed with 4 % paraformaldehyde (Solarbio, Cat. #: P1110, 100 μL/well) for 10 min. The paraformaldehyde was then removed, and the cells were washed twice with 300 μL/well of PBS. A high content analysis system (PerkinElmer) was utilized to capture images and perform the analysis.

2.13. Endotoxin detection

A semi-quantitative detection analysis was performed using the *Limulus* amebocyte lysate (LAL) gel-clot assay prior to immunization, in accordance with *the Pharmacopoeia of the People's Republic of China* (2020, Vol. 4, p. 180). The sensitivity of the *Limulus* lysate reagent (λ) was determined to be 0.125 EU/mL, as provided by Zhanjiang A & C Biological LTD, a subsidiary of Charles River Laboratories International, Inc. The assay was performed following the manufacturer's instructions.

2.14. Mouse immunization

BALB/c mice (Cat. #: 01011) were purchased from Beijing Vital River Animal Technology. C57BL/6 J (Cat. #: C001089) and C57BL/6 J/TLR2 knockout (KO) (Cat. #: C001263) mice were purchased from Cyagen Biosciences. All experiments were approved by the Institutional Animal Care and Use Committee (IACUC) of the Beijing Institute of Biotechnology (approval: DWZX-2024–025). The researchers obtained certificates as laboratory animal practitioners and completed the experiments according to the experimental guidelines.

For intramuscular immunization, mice were randomly divided into four groups, with five mice per group: (1) RBDST (5 μg) + $Al(OH)_3$ (Croda, Cat. #: AJV3012, 100 μg); (2) RBDST (5 μg) + $Al(OH)_3$ (100 μg) + CpG2006 (synthesized by Takara Bio, 50 μg); (3) lipoSC-RBDST (5 μg); and (4) lipoSC-RBDST (5 μg) + $Al(OH)_3$ (100 μg). Mice were immunized with 100 μL of the appropriate treatment on days 0 and 14 via intramuscular injection in the hind leg. Blood samples were

collected 2 weeks after each immunization and centrifuged at 10,000 × g for five minutes to isolate the supernatant, which was collected and stored at −20°C.

For pulmonary delivery, BALB/c mice were randomly divided into five groups, with 13 mice in each group. Before pulmonary delivery, mice were anesthetized with a restraint agent (Beijing Lai Aite Technology, Cat. #: LAT-AFD) at a dose of 200 μL per 10 g of body weight. Each mouse then received a pulmonary delivery of (1) 10 μg of lipoSC-RBDST, while (2) SC-RBDST, (3) RBDST + Pam3CSK4, and (4) lipoSC + RBD were administered at equimolar doses; and (5) a saline group was included as a control. Mice were immunized on days 0, 14, and 28, with each mouse receiving 50 μL per immunization. The serum was isolated from each mouse following the same procedure as described above and tested by an enzyme linked immunosorbent assay (ELISA) for antigen-specific IgG and IgA titers, as well as neutralizing antibody titers. Two weeks after the third immunization, lung tissue from three mice was analyzed by flow cytometry for resident memory T cells, IL-17A cells, and antigen-specific IL-17A, TNF-α, IFN-γ, IL-2, IL-4, and IL-6 levels. For BALF analysis, mice were divided into five groups (as above) with seven mice in each group. Two weeks after the third immunization, samples were collected to measure the antigen-specific IgG and IgA titers, as well as neutralizing antibody titers. C57BL/6 J and C57BL/6 J/*TLR2* KO mice (n = 6) were immunized with 10 μg of lipoSC-RBDST on days 0, 14, and 28. Serum was collected and tested for antigen-specific IgG, IgA, and neutralizing antibody titers, as described above

For intranasal immunization, mice were randomly divided into five groups (n = 5): mice were administered (1) 10 μg of lipoSC-RBDST, while (2) SC-RBDST, (3) RBDST + Pam3CSK4, and (4) lipoSC + RBD were administrated in equal molarity to lipoSC-RBDST, and (5) a saline group was included as a control. Mice were intranasally immunized on days 0, 14, and 28 with 20 μL per injection. Blood samples were collected two weeks after each immunization for serum separation. BALF and nasal lavage fluid (NLF) were collected 2 weeks after the third immunization.

For long-term antibody titer assessment, BALB/c mice were divided into three groups of 10 and immunized via pulmonary delivery of (1) 10 μg of lipoSC-RBDST, (2) an equimolar dose of SC-RBDST, or (3) saline as a control, on days 0, 14, and 28. Serum was collected at two weeks, six months, and eight months post-final dose to assess the IgG, IgA, and neutralizing antibody titers.

For the pulmonary delivery of lipoSC-STXEC to enhance immunity in mice, BALB/c mice were initially immunized intramuscularly in the hind leg with 100 μL of either (1) RBD (10 μg) + $Al(OH)_3$ (100 μg) + CpG2006 (50 μg) or (2) saline on days 0 and 14. One year after the initial intramuscular immunization, lipoSC was conjugated to STXEC at a specific ratio (lipoSC-STXEC), and both lipoSC-STXEC and STXEC were separately administered to the previously immunized mice.

2.15. ELISA

RBD was diluted to 2 μg/mL utilizing coating buffer (50 mmol/L carbonate, pH 9.6), and 100 μL was added to each well of the ELISA plates (Corning, Cat. #: 3590), which were placed at 4°C overnight. The plates were then washed twice with PBST (PBS containing 0.1 % Tween-20), and 300 μL of 5 % skim milk was added to each well before incubating for 1 h at 37°C. Mouse serum was added to the first well and then diluted. The plates were incubated at 37°C for 1 h and then washed three times with PBST. After the 1-h incubation at 37°C, 100 μL of goat anti-mouse IgG (HRP) (Beijing Biodragon Immunotechnologies, Cat. #: BF03001, 1:5000 dilution) or goat anti-mouse IgA alpha chain (HRP) (Abcam, Cat. #: ab97235, 1:10,000 dilution) antibody was added to each well. The plates were then incubated for 1 h at 37°C. Plates were then washed four times with PBST and developed with 100 μL/well of TMB one-component chromogenic solution (Solarbio, Cat. #: PR1200) for 3 min, and 2 M H_2SO_4 (50 μL/well) was added to stop the reaction. The results were measured using microplate reader (SpectraMax® iD3) at 450/630 nm.

2.16. Pseudovirus packaging

HEK293T cells (preserved in our laboratory) were washed twice with PBS, and any remaining liquid was removed by aspiration. Subsequently, 1 mL of trypsin (HyClone, Cat. #: SV30031.01) was added to digest the cells. The digestion reaction was terminated by adding 3 mL of complete DMEM medium, composed of 89 % DMEM (Gibco, Cat. #: C11995500BT), 10 % fetal bovine serum (PAN-Biotech, Cat. #: P30–3306), and 1 % penicillin-streptomycin (Gibco, Cat. #: 15140122). The cells were then plated at a density of 5×10^5 cells/mL in a 10 cm dish and cultured at 37°C in a 5 % CO_2 incubator for 12 h. According to the Lipofectamine 3000 transfection reagent instructions, 7.5 μg of the pNL4–3-R-E backbone plasmid (laboratory stock) and 7.5 μg of SARS-CoV-2 S protein plasmid (synthesized by Sangon Biotech (Shanghai)) were introduced into the cells. After 6–8 h of transfection, the medium was switched to Opti-MEM (Gibco, Cat. #: 31985070). Seventy-two hours post-transfection, the supernatant was collected by centrifuging at 1000 × g for five minutes, passed through a 0.45-μm filter (Pall Corporation, 4614), and stored at −80°C for later use.

2.17. Pseudovirus-neutralization testing

Digested HEK293-ACE2 cells (laboratory stock) were diluted to 2×10^5 cells/mL, and 100 μL of the cell suspension was added to each well of in several 96-well plates (Corning, 3599). The plates were incubated overnight at 37°C with 5 % CO_2. Serum (inactivated at 56°C for 30 min), BALF, or NLF samples were initially diluted with complete DMEM medium. Diluted serum (150 μL) was added to the first well in a row of cell culture plates, followed by three-fold serial dilutions, resulting in five total dilutions per row. For control wells, 100 μL of medium was added to the virus control wells and 150 μL to the cell control wells. Pseudoviruses were diluted to a final concentration of 2×10^4 $TCID_{50}$/mL, and 50 μL of the diluted pseudovirus was added to each sample and virus control well. The plates were gently shaken to mix, and the mixtures were neutralized at 37°C for 1 h. The culture medium from the cells cultured overnight was discarded, and 120 μL of the pseudovirus-serum mixture was transferred to each well containing cells. After 12 h of incubation, the mixture was discarded, and 150 μL of fresh medium was added to each well. The plates were then incubated for an additional 48 h. At the end of the incubation, the plates were equilibrated to 25°C. A total of 100 μL of medium was removed from each well, and 100 μL of reporter gene assay reagent (Vazyme, Cat. #: DD1201) was added. The plates were shaken for two minutes and allowed to react in the dark for five minutes. Subsequently, 100 μL of the reaction mixture was transferred to a CulturPlate-96 white plate (PerkinElmer, Cat. #: 6005290). Fluorescence values were measured utilizing a microplate reader (SpectraMax® iD3).

2.18. Flow cytometry analysis of Tfh and GC B cells in bronchial lymph nodes

BALB/c mice were randomly divided into five groups (five mice per group). Each mouse received 10 μg of lipoSC-RBDST via pulmonary delivery. Both SC-RBDST and lipoSC-RBDST were utilized at equimolar concentrations, and the control group received saline. One week after immunization, bronchoalveolar lymph nodes were collected for flow cytometry to analyze the levels of Tfh and GC B cells. The bronchial lymph nodes of mice were harvested, and a single-cell suspension was prepared following centrifugation and resuspension with staining buffer. The collected cells were stained with anti-CD45 (Invitrogen, Cat. #: 363–0451–82), anti-CD19 (Invitrogen, Cat. #: 414–0193–82), anti-mouse GL7 (BioLegend, Cat. #: 144606), anti-mouse CD95 (Fas) (BioLegend, Cat. #: 152617), anti-mouse CD3 (Invitrogen, Cat. #:

46–0032–82), anti-CD4 (BioLegend, Cat. #: 100529), anti-CD185 (CXCR5) (Invitrogen, Cat. #: 12–7185–80), anti-CD279 (PD-1) (BioLegend, Cat. #: 135218), and anti-CD8a (BD Biosciences, Cat. #: 566985) 25°C for 25 min in the dark. The proportion of Tfh and GC cells was measured using a Cytek® Aurora full spectrum flow cytometer (Cytek Biosciences) and analyzed using SpectroFlo (Cytek, version 3.2.1).

2.19. Flow cytometry analysis of T_{RM} cells in lungs

Fourteen days after the third pulmonary immunization in BALB/c mice, the lungs were mechanically disrupted. The red blood cells were lysed with a buffer and then the sample was centrifuged. The pellet was resuspended in staining buffer, and a single-cell suspension was prepared. A portion of the collected cells was stained with anti-CD45 (Invitrogen, Cat. #: 363–0451–82), anti-CD3 (BD Biosciences, Cat. #: 564009), anti-CD4 (Invitrogen, Cat. #: 414–0042–82), anti-CD8a (BD Biosciences, Cat. #: 566985), anti-CD69 (BioLegend, Cat. #: 104543), and anti-CD103 (BioLegend, Cat. #: 121410), all of which are surface markers. Additionally, anti-IL-17A$^+$ (BioLegend, Cat. #: 506922) was utilized for intracellular antibody staining. T_{RM} cells were measured using a Cytek® Aurora full spectrum flow cytometer (Cytek Biosciences) and was then analyzed using SpectroFlo (Cytek, version 3.2.1).

2.20. Cytokine detection

At 6, 24, 72, and 120 h post-immunization, blood samples were collected from the mice, and serum was further isolated for cytokine analysis. Cytokine concentrations were measured utilizing a Mouse Th1/Th2/Th9/Th17/Th22/Treg Cytokine Panel (17-plex) kit (Cat. #: EPX170–26087–901) from Invitrogen, in accordance with the manufacturer's protocol. The cytokines were measured using a Luminex 200 system.

2.21. Statistical analysis

Statistical analysis was conducted using GraphPad Prism version 10.3.0. Data were expressed as the means ± SD. Data were analyzed by an one-way ANOVA with Dunn's multiple comparison test. Values of $P < 0.05$ were considered to be statistically significant (**** $P < 0.0001$, *** $P < 0.001$, ** $P < 0.01$, and * $P < 0.05$); ns (not significant).

3. Results

3.1. lipoSC-RBDST nanoparticle preparation and characterization

Protein N-terminal lipidation and N-linked glycosylation are two distinct post-translational modification processes in bacterial and eukaryotic cells, both of which rarely occur simultaneously on a protein. The SpyCatcher/SpyTag (SC/ST) system serves as a generic tool for coupling two molecules and makes the modular assembly of nanobioconjugates feasible. The SC/ST system has been broadly used in vaccine development. Here, we prepared N-terminal lipidated SpyCatcher (lipoSC) in *E. coli*, which can be covalently attached to a SpyTag-labeled molecule. In order to elicit RBD-focused immune responses, we selected SARS-CoV-2 RBD delta variant as antigen with SpyTag (ST) genetically fused to the N-terminus (RBDST), and prepared RBDST in glycoengineered *Picha pastoris* with characteristics of glycosylation profile similar to those of mammalian cells [27] (Fig. 1).

Signal peptides from the *E. coli* murein lipoprotein (ML signal peptide),[28] *N. meningitides* Ag473 lipoprotein (Ag signal peptide),[29] *Haemophilus influenzae* P4 outer membrane protein (P4 signal peptide) [30] were separately fused to the N-terminal of SpyCatcher (Figure S1A) and evaluated for the efficiency of directing nascent SpyCatcher peptide to the secretion pathway and then lipidation after localization. The recombinant SpyCatcher (rSC) proteins with distinct signal peptides were expressed as soluble proteins in the supernatant after cell lysis (Figure S1B) and purified from cell lysates via Ni-NTA affinity chromatography in the presence of 1 % Triton X100 in the mobile phase. Although the target bands observed via SDS-PAGE ran slightly lower than 17 kDa (Figure S1B), the size exclusion chromatography (SEC) retention volumes were smaller than that of IgG (~150 kDa) (Superdex™ 200 Increase 10/300 GL, 24 mL total volume, Cytiva) (Figure S1C), suggesting that all three forms of rSC may exist as a multimer.

After that, rSC with the ML signal peptide was selected and further purified by anion exchange chromatography (Source 30Q) and size exclusion chromatography for subsequent experiments. The purified protein displayed a single band via SDS-PAGE (Fig. 2A), indicating high purity. Dynamic light scattering (DLS) analysis indicated that the rSC particle size was approximately 16 nm (Fig. 2B), while transmission electron microscopy (TEM) microscopy revealed that rSC exhibited an irregular granular morphology (Fig. 2C). Edman degradation failed to detect the N-terminal sequence of rSC (data not shown), suggesting that its N-terminus was blocked. To further verify that the N-terminal of rSC was lipidated, we performed LC-MS (TripleTOF 5600, AB Sciex). The molecular weights of rSC proteins were concentrated in two clusters: the first cluster was comprised of molecular weights of 14810.1 Da, 14824.2 Da, and 14838.0 Da, while the second cluster included 14585.8 Da and 14600.0 Da (Fig. 2D). Considering the theoretical molecular weight of unmodified SC protein (13919.11 Da) in conjunction with the theoretical molecular weight of Pam3Cys (910.46 Da), we hyothesized that rSC protein undergoes a fatty acid modification, primarily via triacylation, with a carbon chain length between C16 and C18. Consequently, we designated rSC as lipoSC.

Natural bacterial lipoproteins and synthetic lipopeptides can activate the TLR2-mediated immune signaling pathway.[31] To verify if the lipoSC prepared in this study was able to activate TLR2 downstream signaling, equimolar amounts of lipoSC, Pam3CSK4, and SC were utilized to stimulate TLR2/293T-NFκB-Luc cells, and the relative luciferase activity was measured at various time points. We found that the relative luciferase activity of cells treated with lipoSC and Pam3CSK4 was significantly increased as compared to cells treated with SC (Figure S2A), confirming that the lipoSC prepared in this study has an immunostimulatory function similar to Pam3CSK4. In order to further explore the phagocytosis efficiency of antigen-presenting cells (APCs) towards lipoSC nanoparticles, ST-EGFP was conjugated to lipoSC and used to stimulate macrophages. Compared to ST-EGFP and SC-ST-EGFP, lipoSC-ST-EGFP induced a higher phagocytosis efficiency in macrophages (Fig. 2E), suggesting that lipoSC has the potential to serve as a self-adjuvant carrier protein, aiding in the uptake and presentation of its loaded antigens.

Encouraged by the above results, RBD of the SARS-CoV-2 Delta variant spike protein was fused with SpyTag (RBDST) and conjugated to lipoSC to prepare a bacterial fatty acylated glycoprotein RBD antigen (lipoSC-RBDST). Glycoengineered *P. pastoris*, an expression platform capable of performing mammalian N-glycosylation modifications,[32] was utilized to prepare the SpyTag-labeled glycoprotein RBD antigen (Figure S2B). Consistent with our previous findings,[27] the RBD band shifted downward following PNGase F digestion, indicating the presence of N-glycosylation modifications. Different molar ratios of lipoSC and RBDST were mixed and conjugated at 4°C overnight (12 h), and the optimal ratio for conjugation was determined to be 4:1 (Figure S2C). Unreacted RBDST was removed via size-exclusion chromatography (Figure S2D), resulting in the fatty acylated glycoprotein RBD antigen, lipoSC-RBDST (Fig. 2F). DLS analysis demonstrated that the particle size of lipoSC-RBDST was approximately 16 nm (Figure S2E), with no significant alterations in particle size under storage conditions at 4°C and 37°C and −20°C (Fig. 2G). TEM images revealed that lipoSC-RBDST had an irregular granular morphology (Fig. 2H). Taken together, these study findings confirmed the successful construction of the

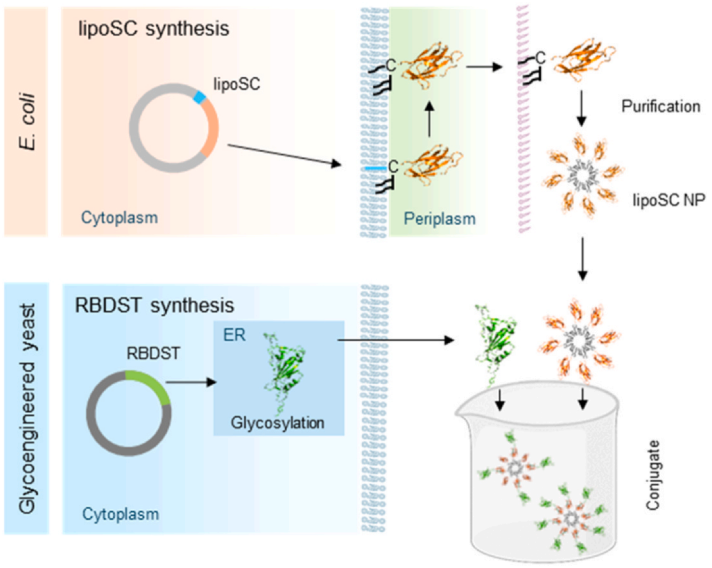

Fig. 1. Modular construction of the bacterial lipidation-based SARS-CoV-2 mucosal nanovaccine.

bacterial fatty acylated SARS-CoV-2 glycoprotein RBD antigen lipoSC-RBDST through SC/ST conjugation.

3.2. LipoSC-RBDST effectively induces humoral immune responses

Following the preparation of lipoSC-RBDST, a semi-quantitative detection analysis was conducted using the *Limulus* amebocyte lysate (LAL) gel-clot assay prior to immunization, in accordance with the *Pharmacopoeia of the People's Republic of China* (2020, Vol. 4, p. 180). We found that the endotoxin concentration in the sample was approximately 125 EU/mL (Figure S3A). Our previous studies showed that the combination of $Al(OH)_3$ and CpG2006 adjuvants significantly increased the immunogenicity and protective efficacy of RBD vaccines.[33,34] To investigate if fatty acylation could enhance the immunogenicity of RBD, we evaluated the ability of lipoSC-RBDST to induce binding and neutralizing antibodies upon intramuscular immunization. Seven-week-old BALB/c mice were randomly divided into four groups (n = 5) and intramuscularly immunized with 5 μg RBDST twice at a 14-day interval in the following formulations: RBDST + $Al(OH)_3$, RBDST + $Al(OH)_3$ + CpG2006, lipoSC-RBDST, and lipoSC-RBDST + $Al(OH)_3$ (Figure S3B). The results demonstrated that a single dose of lipoSC-RBDST stimulated high titers of RBD-binding antibodies, regardless of the presence of $Al(OH)_3$ (Figure S3C). When combined with $Al(OH)_3$, neutralizing antibodies with a titer of 1:182 were induced (Figure S3D). After a second immunization, RBDST + $Al(OH)_3$ + CpG2006, lipoSC-RBDST, and lipoSC-RBDST + $Al(OH)_3$ all induced neutralizing antibodies with titers above 10^3 (Figure S3D). Taken together, these findings suggest that fatty acylation substantially enhances RBD immunogenicity and the induction of neutralizing antibodies.

3.3. Aerosolized lipoSC-RBDST administered via the pulmonary route exhibits high safety and efficient induction of immune responses

After establishing the humoral immunogenicity of lipoSC-RBDST, we further investigated its capacity to induce respiratory mucosal immune responses. We assessed the safety of pulmonary delivery of aerosolized lipoSC-RBDST (Fig. 3A). Seven-week-old BALB/c mice were randomly divided into three groups (n = 5) and subjected to pulmonary delivery of aerosolized saline, SC-RBDST, or lipoSC-RBDST, with each mouse receiving 10 μg of protein (Fig. 3A). The body weight, body temperature, and cytokine (TNF-α, IL-1β, IL-6) levels were determined in each mouse. Post-immunization, the mice maintained body temperatures between 36°C and 37°C (Fig. 3B). The body weight of the mice declined at 24 h, probably due to anesthesia, but then gradually recovered, with no significant differences between immunization and saline groups (Fig. 3C). At 6 h post-immunization, TNF-α levels in the lipoSC-RBDST group were slightly elevated, IL-6 levels were significantly increased in both SC-RBDST and lipoSC-RBDST groups, and IL-1β generally remained unchanged (Fig. 3D). These data imply that aerosolized lipoSC-RBDST administered via the pulmonary route is safe and does not induce severe adverse effects. The proportions of Tfh and germinal center (GC) B cells are critical indicators of adaptive immune responses. Seven days post-immunization, bronchial draining lymph nodes were isolated to detect the proportions of Tfh and GC B cells. We found that the proportions of Tfh and GC B cells in the bronchial lymph nodes of the lipoSC-RBDST group were significantly elevated as compared to those in the saline and SC-RBDST groups (Fig. 3E), suggesting that lipoSC-RBDST induces significant adaptive immune responses.

3.4. Aerosolized lipoSC-RBDST administered via the pulmonary route induces RBD-specific humoral and mucosal immune responses

After confirming the safety and immunogenicity of aerosolized lipoSC-RBDST delivered via the pulmonary route, we evaluated its protective efficacy and ability to stimulate RBD-specific antibody responses. BALB/c mice were randomly divided into five groups (n = 10). The lipoSC-RBDST group was immunized with 10 μg of total protein, while the SC-RBDST, RBDST + Pam3CSK4, and lipoSC + RBD groups received equimolar amounts of RBD and Pam3CSK4 or lipoSC. The saline group served as the negative control. All groups received three doses, with a 14-day interval between each dose (Fig. 4A). The results demonstrated that a single immunization with aerosolized lipoSC-RBDST induced RBD-specific IgG in the serum, while the second immunization induced RBD-specific IgA in the serum. After the third immunization, the lipoSC-RBDST group achieved RBD-specific IgG and IgA titers of 1:912011 and 1:4677, respectively, which were significantly higher than those in the lipoSC + RBD group (Fig. 4B, C). A pseudovirus neutralization assay, which is widely utilized to assess the protective efficacy of COVID-19 vaccines, demonstrated that two doses of either lipoSC-RBDST or lipoSC + RBD induced detectable neutralizing antibodies in the serum. After three doses, the lipoSC-RBDST group achieved a neutralizing antibody titer of 1:9333, which was substantially higher than that found in the lipoSC + RBD group. No neutralizing antibodies were detected in the saline, SC-RBDST, or RBDST + Pam3CSK4 groups (Fig. 4D). In contrast, immunization of C57BL/6 J *TLR2*-knockout mice with aerosolized lipoSC-RBDST induced lower serum levels of RBD-specific IgG (Figures S4A, B), IgA (Figure S4C), and neutralizing antibodies (Figure S4D),

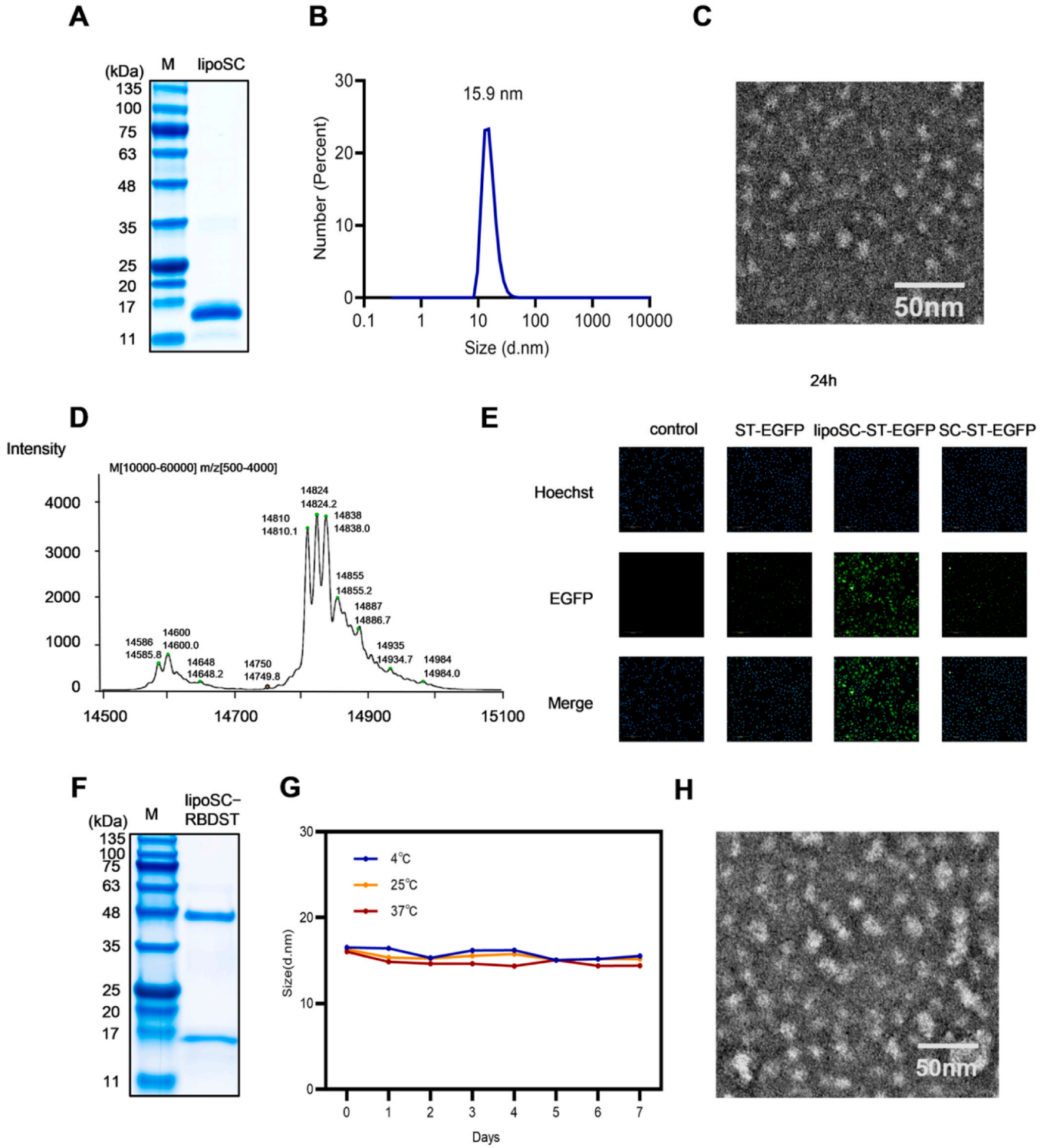

Fig. 2. Preparation and characterization of the nanoparticle antigen lipoSC-RBDST. A) Coomassie blue staining of lipoSC nanoparticles after separation via size-exclusion chromatography (Superdex™ 200 Increase 10/300 GL, 24 mL total volume). B) Dynamic light scattering analysis of lipoSC nanoparticles. C) A transmission electron microscopy image showing the morphology of purified lipoSC nanoparticles. D) Liquid chromatography-mass spectrometry (TripleTOF 5600, AB Sciex) analysis of the molecular weight of lipoSC. E) Fluorescence imaging of macrophages stimulated with the complex formed by lipoSC and SpyTag-labeled EGFP. F) Coomassie blue staining analysis of the covalent complex formation between lipoSC and RBDST. G) Dynamic light scattering analysis of the stability of lipoSC-RBDST after storage at 4°C, 25°C and 37°C for 7 days. H) A transmission electron microscopy image showing the morphology of lipoSC-RBDST nanobioconjugates.

indicating that lipoSC-RBDST enhanced the immune response through the TLR2-mediated signaling pathway. To investigate if immunization via the pulmonary route induces mucosal antibody responses, bronchoalveolar lavage fluid (BALF) was collected two weeks after the third immunization in order to assess RBD-specific IgG, IgA, and neutralizing antibody titers. The lipoSC-RBDST group achieved IgG, IgA, and pseudovirus neutralizing antibody titers of 1:6026 (Figs. 4E), 1:3236 (Figs. 4F), and 1:309 (Fig. 4G), respectively, all of which were significantly higher than those in the other groups. To evaluate the durability of RBD-specific antibodies induced by immunization via the

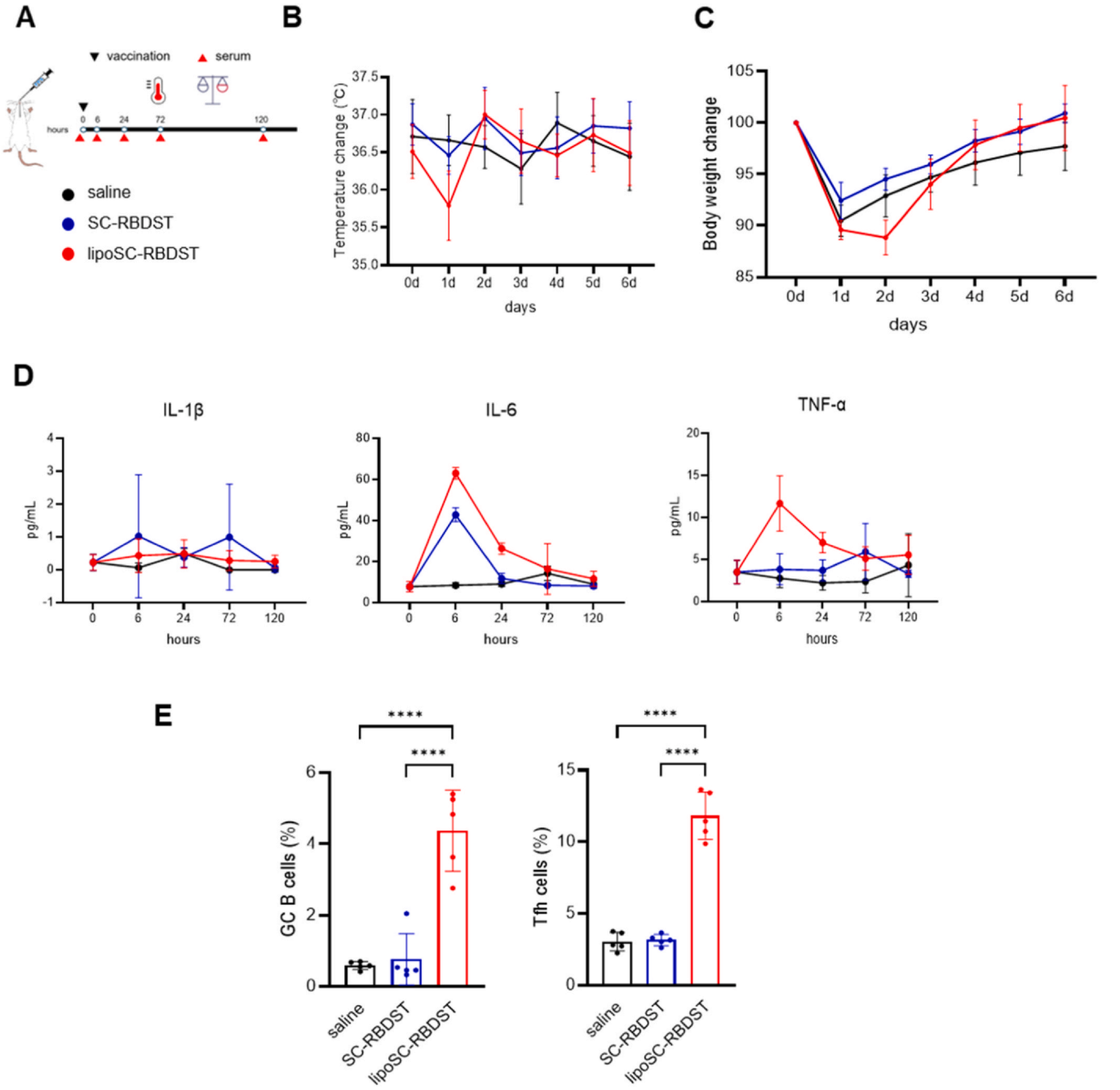

Fig. 3. Evaluation of the safety and humoral immune response induced by lipoSC-RBDST delivered via the pulmonary route. A) Immunization schedule for assessing the safety of lipoSC-RBDST. Body weight (B) and body temperature (C) of BALB/c mice immunized with lipoSC-RBDST via the pulmonary route. D) Serum levels of inflammatory cytokines IL-1β, IL-6, and TNF-α at various time points after a single immunization with lipoSC-RBDST. E) Proportions of GC B cells ($GL7^+$ $CD95^+$ cells among the $CD19^+$ cells) and Tfh cells ($CXCR5^+$ $PD1^+$ cells among the $CD4^+$ T cells) in the bronchial lymph nodes 7 days post vaccination as determined by flow cytometry (n = 5).

pulmonary route, serum IgG (Figure S4E), IgA (Figure S4F), and neutralizing antibody (Figure S4G) titers were measured eight months after the final immunization and were found to be 1:50119, 1:4169, and 1:1259, respectively, with no substantial decline observed.

Respiratory tract tissue-resident memory T cells (T_{RM}) play an essential role in mucosal immune protection.[35,36] To determine whether lipoSC-RBDST induces T_{RM}, the lungs of mice were collected 14 days after the last immunization and dissociated into single-cell suspensions (n = 3). Flow cytometry was employed to evaluate the proportions of $CD69^+$ $CD103^+$ $CD4^+$ T cells, $CD69^+$ $CD103^+$ $CD8^+$ T cells, and $IL\text{-}17A^+$ $CD4^+$ T cells in the lung tissue. We found that the lipoSC + RBD and lipoSC-RBDST groups displayed elevated proportions of all three T cells in the lungs as compared to the saline, SC-RBDST, and RBDST + Pam3CSK4 groups (Fig. 4H), indicating that lipoSC induces local cellular immune responses in the lung.

3.5. LipoSC-RBDST stimulates strong humoral and mucosal immune responses in mice via intranasal immunization

To further confirm the ability of lipoSC-RBDST to induce respiratory mucosal immune responses, we assessed the induction of RBD-specific IgG, IgA, and neutralizing antibodies by intranasal immunization using the same regimen as that employed for pulmonary immunization (Fig. 5A). The lipoSC-RBDST group exhibited serum IgG and IgA titers

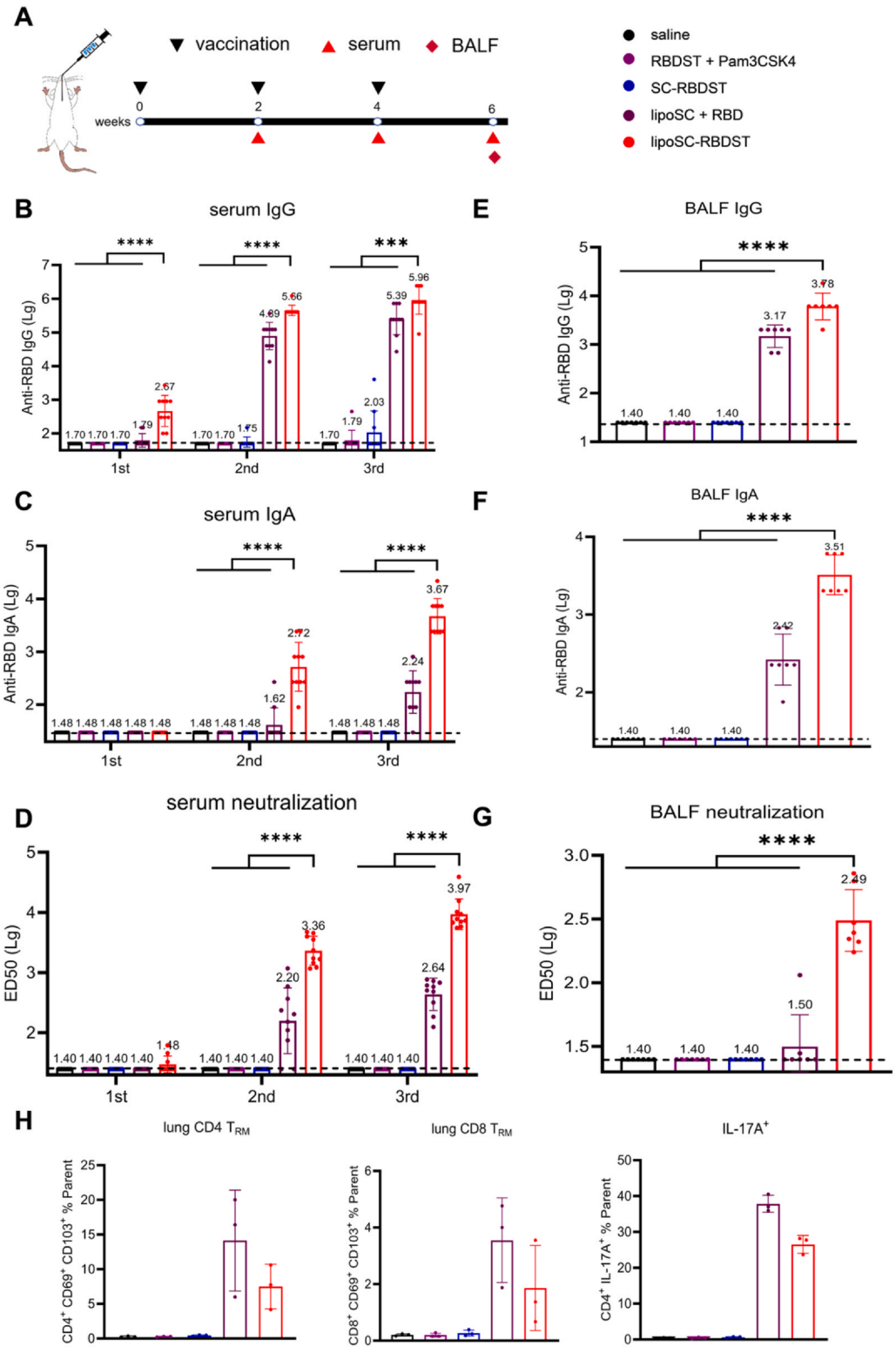

Fig. 4. Immunization with aerosolized lipoSC-RBDST via the pulmonary route effectively induces mucosal and humoral immune responses in BALB/c mice. A) Immunization schedule for evaluating the efficacy of aerosolized lipoSC-RBDST delivered via the pulmonary route in BALB/c mice. SARS-CoV-2 RBD-specific IgG titers (B), IgA titers (C), and neutralizing antibody titers (D) in the serum 14 days after three doses of saline, RBDST + Pam3CSK4, SC-RBDST, lipoSC + RBD, or lipoSC-RBDST (n = 10). RBD-specific IgG titers (E), IgA titers (F), and neutralizing antibody titers (G) in the bronchoalveolar lavage fluid following immunization with lipoSC-RBDST via the pulmonary route (n = 7). H) Analysis of T cells 14 days after three doses of lipoSC-RBDST were given via the pulmonary route, including CD4 tissue-resident memory T cells ($CD69^+$ $CD103^+$ $CD4^+$ T cells), CD8 tissue-resident memory T cells ($CD69^+$ $CD103^+$ $CD8^+$ T cells), and IL-17-secreting tissue-resident memory T cells ($IL\text{-}17A^+$ $CD4^+$ T cells) (n = 3).

of 1:467735 and 1:2042, respectively, which were significantly increased as compared to those of the lipoSC + RBD group. No antibody titers were detected in the SC-RBDST group (Fig. 5B, C). A pseudovirus neutralization assay demonstrated that two doses of intranasal lipoSC-RBDST stimulated a serum neutralizing antibody titer of 1:162, which increased to 1:933 after three doses—significantly higher than the lipoSC + RBD group (Fig. 5D). Two weeks after the third immunization, BALF and nasal lavage fluid (NLF) were collected from all groups to detect RBD-specific antibody titers. The lipoSC-RBDST group showed IgG and IgA titers of 1:3890 and 1:537 in BALF, both significantly higher than those of other groups (Fig. 5E, F), while IgG and IgA titers in NLF were both 1:117 (Fig. 5H, I). However, the positive conversion rates and titers of neutralizing antibodies in BALF and NLF were relatively low (Fig. 5G, J). These results indicate that immunization with lipoSC-RBDST via the upper respiratory tract can also induce significant mucosal and humoral immune responses.

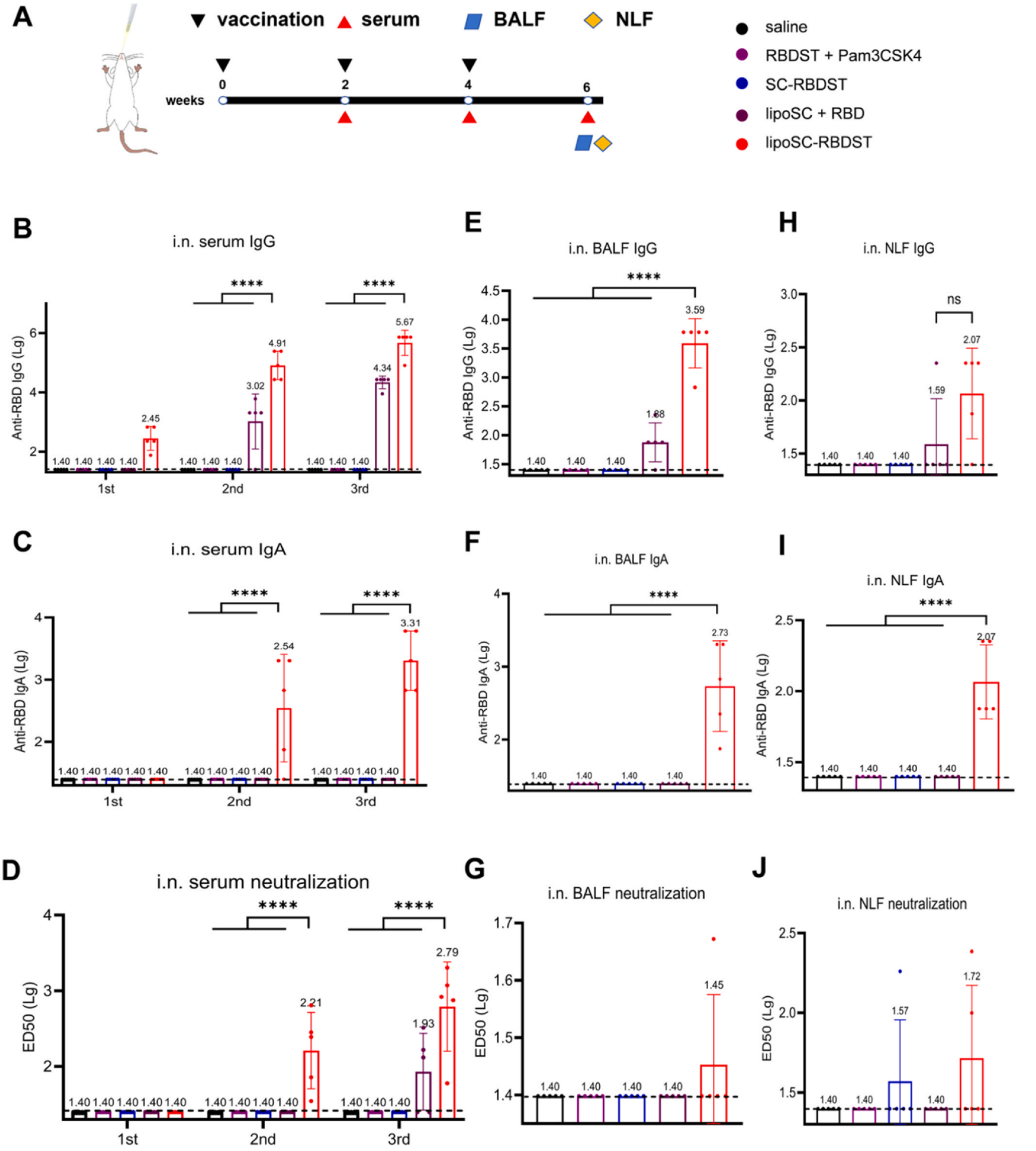

Fig. 5. Intranasal immunization with lipoSC-RBDST effectively induces mucosal and humoral immune responses in BALB/c mice. A) Immunization schedule for evaluating the efficacy of lipoSC-RBDST via intranasal administration in BALB/c mice. SARS-CoV-2 RBD-specific IgG titers (B), IgA titers (C), and neutralizing antibody titers (D) in the serum 14 days after three doses of saline, RBDST + Pam3CSK4, SC-RBDST, lipoSC + RBD, or lipoSC-RBDST (n = 5). RBD-specific IgG titers (E), IgA titers (F), and neutralizing antibody titers (G) in the bronchoalveolar lavage fluid. RBD-specific IgG titers (H), IgA titers (I), and neutralizing antibody titers (J) in nasal lavage fluid.

3.6. Mucosal booster immunization with lipoSC-STXEC effectively induces robust variant-specific neutralizing antibodies in mice with pre-existing immunity to wild-type RBD (RBD_{WT})

In order to explore if pre-existing immunity enhances mucosal heterologous booster immunization with a fatty acylated variant RBD to induce mucosal immune responses against the variant, we utilized the RBD of the SARS-CoV-2 XEC variant, which exhibits elevated transmissibility and immune evasion capacity,[37] as the antigen to prepare lipoSC-STXEC. Antibody responses against the variant were evaluated in mice with pre-existing immunity to the wild-type RBD (RBD_{WT}) following immunization with aerosolized lipoSC-STXEC via the

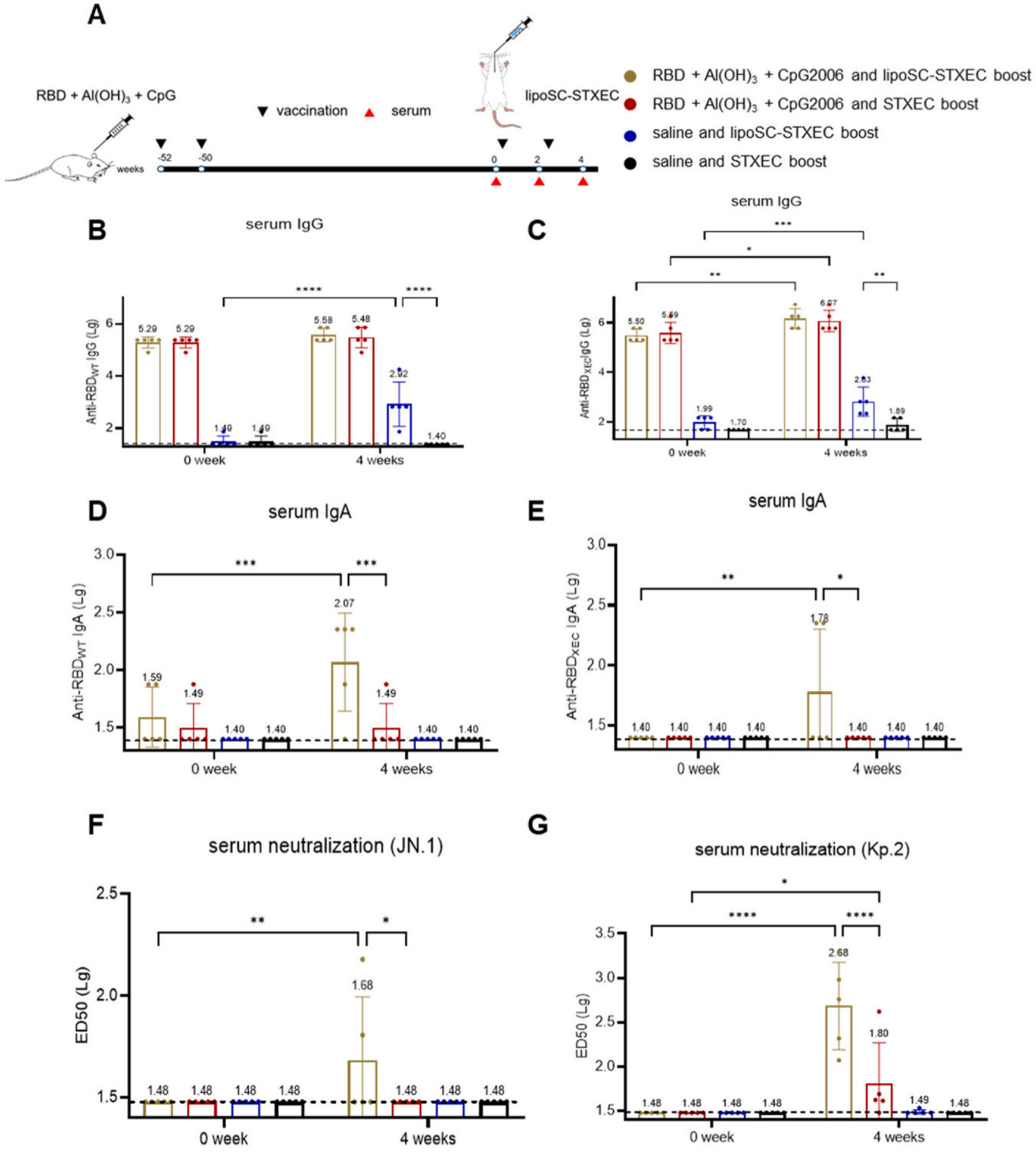

Fig. 6. Evaluation of the efficacy of booster immunization with aerosolized lipoSC-STXEC via the pulmonary route in mice previously immunized intramuscularly with wild-type RBD. A) The schedule for booster immunization with aerosolized lipoSC-STXEC via the pulmonary route in mice previously immunized intramuscularly with wild-type RBD. RBD_{WT}-specific (B) and RBD_{XEC}-specific (C) IgG titers in the serum before and after lipoSC-STXEC booster immunization. RBD_{WT}-specific (D) and RBD_{XEC}-specific (E) IgA titers in the serum before and after lipoSC-STXEC booster immunization. Neutralizing antibody titers against JN.1 (F) and Kp.2 (G) in the serum before and after lipoSC-STXEC booster immunization.

pulmonary route. BALB/c mice were immunized twice via intramuscular injection with RBD_{WT} + $Al(OH)_3$ + CpG2006 at a 14-day interval. After 50 weeks, the mice received two pulmonary immunizations with either lipoSC-STXEC or STXEC, and then the serum titers of IgG, IgA, and neutralizing antibodies against RBD_{WT} and RBD_{XEC} were determined (Fig. 6A). Fifty weeks after receiving two doses of RBD_{WT} + $Al(OH)_3$ + CpG2006, the mice maintained detectable levels of RBD_{WT}-specific (Fig. 6B) and RBD_{XEC}-specific (Fig. 6C) IgG in the serum. However, both RBD_{WT}-specific (Fig. 6D) and RBD_{XEC}-specific (Fig. 6E) IgA titers remained at low levels, and no neutralizing antibody activity was observed against JN.1 (Fig. 6F) or Kp.2 (Fig. 6G). Following pulmonary delivery of lipoSC-STXEC, RBD_{XEC}-specific IgG titers

increased substantially in the serum (Fig. 6C), along with elevated titers against RBD_{WT}-specific (Fig. 6D) and RBD_{XEC}-specific (Fig. 6E) IgA. Notably, the titer of neutralizing antibodies against Kp.2, which is phylogenetically close to XEC, exhibited marked elevation. In contrast, mice lacking RBD_{WT} pre-existing immunity failed to induce immune responses against the variant. Moreover, even in the presence of RBD_{WT} pre-existing immunity, a non-fatty acylated antigen was unable to induce immune responses against the variant.

4. Discussion

SARS-CoV-2 mainly disseminates through the respiratory tract.[38] Although intramuscular vaccines are effective in decreasing severe disease outcomes and mortality, they do not induce mucosal immunity, emphasizing the necessity for the development of mucosal vaccines. The currently approved COVID-19 mucosal vaccines primarily use viral vectors,[39] which may suffer from reduced efficacy due to pre-existing immunity.[22] In contrast, subunit vaccines, which are known for their well-defined structure and favorable safety profile,[40] bypass the issue of pre-existing immunity. However, their limited immunogenicity poses a challenge in inducing strong mucosal immune responses, necessitating strategies to improve their immunogenic potential. Fatty acylated antigens have the potential to act as TLR2 agonists, thereby increasing immune responses while circumventing pre-existing immunity. Given that fatty acylation is a modification specific to bacteria, and the glycosylation of the RBD is critical to maintaining structural stability and immunogenicity,[41] we utilized a modular assembly strategy to facilitate the fatty acylation of glycosylated antigens. Specifically, we expressed fatty acylated SC in *E. coli*, produced glycosylated RBD in glycoengineered *P. pastoris*, and took advantage of the ability of the SC/ST system to form isopeptide bonds in vitro to facilitate the modular assembly of fatty acylated and glycosylated antigens.

The expression of lipoSC in *E. coli* was analyzed by comparing the expression levels of the recombinant Ag473 protein (rAg473), which is directed by the *N. meningitidis* lipoprotein signal peptide, in *E. coli* strains BL21(DE3) and C43(DE3). The C43(DE3) strain exhibited superior protein expression as compared to BL21(DE3). N-terminal sequencing of purified rAg473 utilizing Edman degradation found that rAg473 from BL21(DE3) started with an MKKL sequence, indicating incomplete lipidation. In contrast, the N-terminus of rAg473 from C43(DE3) was not able to be sequenced, indicating that post-translational modifications obstructed the N-terminus. Mass spectrometry analysis confirmed the appropriate lipid modification of purified rAg473.[42] Therefore, the *E. coli* C43(DE3) strain was deemed more suitable for expressing fatty acylated antigens in this study. Nonetheless, further research is warranted in order to explore the variations in the type of fatty acid modifications on the SC system across various expression strains.

As of now, Trumenba® (rLP2086), a lipoprotein-based vaccine developed by Pfizer that received FDA approval in 2014, is the only lipoprotein-based vaccine targeting Group B *N. meningitidis*,. Intranasal administration of rLP2086 in murine models has been shown to diminish nasal colonization by *N. meningitidis*,[43] thereby demonstrating its efficacy in eliciting mucosal immunity. However, the rLP2086 produced in *E. coli* lacks glycosylation modifications. In contrast, our previous study employed glycoengineered *P. pastoris* to produce the RBD with mammalian-like glycosylation, presenting a cost-effective strategy amenable to high-density fermentation.[27] By leveraging the capability of the SC/ST system to form stable isopeptide bonds *in vitro*, we successfully conjugated fatty acylated RBD antigens. This methodology permits the independent expression of the nanocarrier and antigen in optimized expression systems, thereby ensuring high yield and purity for both components. The resultant lipoSC nanoparticles, approximately 16 nm in diameter, are likely formed due to the fatty acid chains creating a hydrophobic core, while the hydrophilic peptide domains on the exterior facilitate nanoparticle assembly. This nanocarrier aids the presentation of a variety of antigens on its surface, and the orthogonal conjugation strategy employed herein enhances the expedited development of nanovaccines.

At 6 h post-immunization, we observed a slight elevation in TNF-α levels in the lipoSC-RBDST group, while IL-6 levels were significantly increased in both the SC-RBDST and lipoSC-RBDST groups. These cytokine elevations were transient, with both IL-6 and TNF-α levels returning to baseline within 24 h post-immunization (Fig. 3D). These data suggest that lipoSC-RBDST vaccine administered via the pulmonary route is safe in the short term and does not induce severe adverse effects, indicating that the vaccine platform is safe and well-tolerated in the mouse model. Although the transient increase in cytokines warrants further investigation, we believe that these immune responses do not compromise the safety of the vaccine in the short term. However, future studies should address the potential long-term implications of these cytokine elevations, particularly in populations with pre-existing inflammatory conditions. IL-6 and TNF-α are key pro-inflammatory cytokines,[44,45] and while the elevations observed here were brief, their impact on immune responses may vary in individuals with underlying conditions, such as the elderly or those with compromised immune systems. Therefore, it is important to assess the dynamics of cytokine levels and their potential effects on immune responses in these specific populations in future clinical studies.

In this study, mucosal immunization with lipoSC-RBDST induced robust mucosal and humoral immune responses in mice, whereas the RBD + Pam3CSK4 group did not induce an effective immune response, consistent with findings from prior studies. Previous research has demonstrated that the N-terminal fragment of the recombinant lipoprotein rlipo-D1E3, produced via trypsin cleavage and referred to as lipo-Nter, displays superior anti-tumor effects as compared to synthetic lipopeptides.[46] Vaccination of mice with a recombinant HPV16 E7 mutant protein (rE7m) in conjunction with lipo-Nter resulted in increased levels of anti-E7 antibodies, and a single administration of rE7m with lipo-Nter inhibited tumor growth, whereas rE7m alone had no effect. Similarly, lipo-Nter improved the anti-tumor efficacy of E7-based peptide vaccines, in contrast to Pam3CSK4, which did not. These findings highlight the potential of the recombinant lipoprotein lipo-Nter as a potent novel adjuvant, offering significant promise for the development of next-generation subunit vaccines, while underscoring the limited efficacy of Pam3CSK4. The strong mucosal and humoral immune responses stimulated by lipoSC-RBDST can be ascribed to several factors. First, it functions as a TLR2 receptor agonist, thus activating immune signaling pathways. Second, its nanoparticle architecture enhances efficient antigen presentation by APCs. Finally, the intramolecular adjuvant design likely enables the concurrent targeting of the antigen and adjuvant to the same cell, thus amplifying the immune response.

Adenoviral vector-based vaccines, such as Ad5 and ChAd platforms, have been widely used for mucosal immunization due to their ability to generate strong immune responses.[47,48] However, these vaccines often face challenges, including pre-existing immunity to the adenoviral vector, immune-mediated inflammation, and limitations in repeated dosing.[22,49,50] In contrast, protein-based nanoparticle vaccines are typically safer, with fewer concerns regarding pre-existing immunity, and can precisely display antigens. However, they often require the use of additional adjuvants to achieve robust mucosal immune responses. The lipoSC scaffold allows for efficient mucosal delivery and antigen uptake by APCs without the need for viral vectors. Furthermore, conjugating RBDST to the lipoSC system facilitates precise antigen presentation and induces strong mucosal IgA and systemic antibody responses, as well as T_{RM} formation.

The *in vitro* data confirmed that lipoSC activates TLR2 signaling and significantly enhances antigen uptake by APCs. In the context of respiratory mucosal vaccination, lung-resident DCs, particularly the $CD103^+$ DC subset, play a pivotal role in capturing luminal antigens and migrating to draining lymph nodes to prime adaptive immunity.[17] It is highly likely that the lipidated moiety of lipoSC-RBDST acts as a

ligand for TLR2 on these mucosal DCs, triggering their maturation and enhancing antigen presentation efficacy. This potent DC activation is crucial for driving the subsequent adaptive responses we observed. Specifically, TLR2-activated DCs are known to create a cytokine milieu favorable for the differentiation of Tfh cells, which we found elevated in bronchial lymph nodes. These Tfh cells are essential for promoting GC B cell responses and subsequent class switching to sIgA, consistent with the high levels of RBD-specific sIgA detected in BALF and NLF. Furthermore, TLR2 signaling has been implicated in promoting Th17 cell differentiation.[51] The observed increase in lung-localized IL-17A$^+$ CD4$^+$ T cells and T_{RM} cells suggests that lipoSC-RBDST may drive a TLR2-dependent Th17-T_{RM} axis, which is vital for establishing rapid, frontline protection at mucosal surfaces. While definitive characterization of the phenotypes and kinetics of these specific lung DC subsets and T-cell differentiation pathways awaits future *in vivo* tracking studies, the integration of our current data strongly points to these coordinate cellular events as the basis for the vaccine's potent mucosal immunogenicity.

This study has several limitations. First, flow cytometry analysis of lung-T_{RM} cells in mice following pulmonary immunization revealed that lipoSC-RBDST effectively induces T_{RM} formation. To elucidate the vaccine's mechanism of action more thoroughly, future research should utilize fluorescent labeling techniques to monitor the distribution, retention time, and diffusion of vaccine antigens into surrounding tissues. This approach would aid the assessment of the utilization efficiency of fatty acylated nanoparticle vaccines. Furthermore, flow cytometry should be employed to quantify the proportion of antigen-specific memory B cells within peripheral blood mononuclear cells. A comprehensive analysis of these data, including aspects of antigen presentation, immune cell activation, and antigen-specific B cell activation, would yield profound insights into the mechanisms underlying the vaccine's immune response. Thirdly, this study evaluated vaccine efficacy exclusively through upper and lower respiratory mucosal immunization. Further optimization of nebulization devices is necessary to improve vaccine performance. Fourthly, while the 41 % conjugation efficiency for lipoSC-RBDST confirms effective site-specific lipidation, we recognize the need for improvements in scalability and reproducibility. Future strategies may involve optimizing reaction parameters (e.g., pH, temperature, shortening induction times), or imodifying the construct design by inserting the SpyTag sequence at the N-terminus of the RBD protein to mitigate potential degradation. Another limitation of this study is the lack of direct *in vivo* protective efficacy data against viral challenge. Although the high neutralizing antibody titers observed strongly suggest potential protection, confirmation in a live virus challenge model was not feasible in the current setup due to biosafety facility constraints. Lastly, as a versatile nanocarrier, the applicability and efficacy of lipoSC should be examined for antigens derived from other bacterial or viral pathogens.

5. Conclusion

In summary, this study demonstrates an innovative strategy for mucosal vaccine design by integrating bacterial N-terminal fatty acylation into a glycosylated RBD. LipoSC synergistically enhances the immunogenicity of RBD by acting as both a self-assembling scaffold and an intramolecular adjuvant, which in turn elicited robust mucosal and humoral immune responses in murine models. This approach effectively circumvents the challenge of pre-existing immunity associated with viral vectors. This methodology offers both essential theoretical foundation and empirical data for the design and development of mucosal vaccines, especially through innovative strategies aimed at enhancing antigen immunogenicity and optimizing antigen delivery. This study serves as a valuable reference for the advancement of next-generation COVID-19 mucosal vaccines and provides insights applicable to the broader development of respiratory mucosal vaccines.

CRediT authorship contribution statement

Yanru Zhang: Methodology. **Han Wang:** Methodology. **Shujuan Yu:** Methodology. **Xuchen Hou:** Methodology. **Bin Zhang:** Methodology. **Peng Sun:** Writing – review & editing, Writing – original draft, Methodology, Formal analysis, Conceptualization. **Jun Wu:** Writing – review & editing, Formal analysis, Conceptualization. **Bo Liu:** Writing – review & editing, Formal analysis, Conceptualization. **Huifang Xu:** Writing – original draft, Methodology, Formal analysis, Data curation, Conceptualization. **Tiantian Wang:** Writing – review & editing.

Declaration of Competing Interest

All authors have approved the submission. There are no conflicts to declare.

Appendix A. Supporting information

Supplementary data associated with this article can be found in the online version at doi:10.1016/j.glycos.2025.100019.

References

1. Huang C, et al. Clinical features of patients infected with 2019 novel coronavirus in Wuhan, China. *Lancet.* 2020;395:497–506. https://doi.org/10.1016/S0140-6736(20)30183-5
2. SeyedAlinaghi S, et al. Characterization of SARS-CoV-2 different variants and related morbidity and mortality: a systematic review. *Eur J Med Res.* 2021;26:51. https://doi.org/10.1186/s40001-021-00524-8
3. Watson OJ, et al. Global impact of the first year of COVID-19 vaccination: a mathematical modelling study. *Lancet Infect Dis.* 2022;22:1293–1302. https://doi.org/10.1016/S1473-3099(22)00320-6
4. Wang H, et al. Development of an inactivated vaccine candidate, BBIBP-CorV, with potent protection against SARS-CoV-2. *Cell.* 2020;182:713–721. https://doi.org/10.1016/j.cell.2020.06.008 e719.
5. Xin Q, et al. Efficacy, immunogenicity and safety of CoronaVac(R) in children and adolescents aged 6 months to 17 years: a multicenter, randomized, double-blind, placebo-controlled phase III clinical trial. *Nat Commun.* 2024;15:6660. https://doi.org/10.1038/s41467-024-50802-2
6. Bettini E, Locci M. SARS-CoV-2 mRNA vaccines: immunological mechanism and beyond. *Vaccines.* 2021;9. https://doi.org/10.3390/vaccines9020147
7. Mendonca SA, Lorincz R, Boucher P, Curiel DT. Adenoviral vector vaccine platforms in the SARS-CoV-2 pandemic. *npj Vaccin.* 2021;6:97. https://doi.org/10.1038/s41541-021-00356-x
8. Zhu FC, et al. Immunogenicity and safety of a recombinant adenovirus type-5-vectored COVID-19 vaccine in healthy adults aged 18 years or older: a randomised, double-blind, placebo-controlled, phase 2 trial. *Lancet.* 2020;396:479–488. https://doi.org/10.1016/S0140-6736(20)31605-6
9. Heidary M, et al. A comprehensive review of the protein subunit vaccines against COVID-19. *Front Microbiol.* 2022;13:927306. https://doi.org/10.3389/fmicb.2022.927306
10. Dai L, et al. Efficacy and safety of the RBD-dimer-based Covid-19 vaccine ZF2001 in adults. *N Engl J Med.* 2022;386:2097–2111. https://doi.org/10.1056/NEJMoa2202261
11. Hassan AO, et al. A single-dose intranasal ChAd vaccine protects upper and lower respiratory tracts against SARS-CoV-2. e113 *Cell.* 2020;183:169–184. https://doi.org/10.1016/j.cell.2020.08.026
12. Xing M, et al. An intranasal combination vaccine induces systemic and mucosal immunity against COVID-19 and influenza. *npj Vaccin.* 2024;9:64. https://doi.org/10.1038/s41541-024-00857-5
13. Tsai CJY, Loh JMS, Fujihashi K, Kiyono H. Mucosal vaccination: onward and upward. *Expert Rev Vaccin.* 2023;22:885–899. https://doi.org/10.1080/14760584.2023.2268724
14. Lee S, Yeung KK, Watts TH. Tissue-resident memory T cells in protective immunity to influenza virus. *Curr Opin Virol.* 2024;65:101397. https://doi.org/10.1016/j.coviro.2024.101397
15. Pilapitiya D, Wheatley AK, Tan HX. Mucosal vaccines for SARS-CoV-2: triumph of hope over experience. *EBioMedicine.* 2023;92:104585. https://doi.org/10.1016/j.ebiom.2023.104585
16. Lavelle EC, Ward RW. Mucosal vaccines - fortifying the frontiers. *Nat Rev Immunol.* 2022;22:236–250. https://doi.org/10.1038/s41577-021-00583-2
17. Ye T, et al. Inhaled SARS-CoV-2 vaccine for single-dose dry powder aerosol immunization. *Nature.* 2023;624:630–638. https://doi.org/10.1038/s41586-023-06809-8
18. Mao T, et al. Unadjuvanted intranasal spike vaccine elicits protective mucosal immunity against sarbecoviruses. *Science.* 2022;378:eabo2523. https://doi.org/10.1126/science.abo2523
19. Park YJ, et al. Imprinted antibody responses against SARS-CoV-2 Omicron sublineages. *Science.* 2022;378:619–627. https://doi.org/10.1126/science.adc9127

20. Kurhade C, et al. Low neutralization of SARS-CoV-2 Omicron BA.2.75.2, BQ.1.1 and XBB.1 by parental mRNA vaccine or a BA.5 bivalent booster. *Nat Med.* 2023;29:344–347. https://doi.org/10.1038/s41591-022-02162-x
21. Johnston TS, et al. Immunological imprinting shapes the specificity of human antibody responses against SARS-CoV-2 variants. e914 *Immunity.* 2024;57:912–925. https://doi.org/10.1016/j.immuni.2024.02.017
22. Zhu FC, et al. Safety, tolerability, and immunogenicity of a recombinant adenovirus type-5 vectored COVID-19 vaccine: a dose-escalation, open-label, non-randomised, first-in-human trial. *Lancet.* 2020;395:1845–1854. https://doi.org/10.1016/S0140-6736(20)31208-3
23. Wang WC, Sayedahmed EE, Mittal SK. Significance of Preexisting Vector Immunity and Activation of Innate Responses for Adenoviral Vector-Based Therapy. *Viruses.* 2022;14. https://doi.org/10.3390/v14122727
24. Jin MS, et al. Crystal structure of the TLR1-TLR2 heterodimer induced by binding of a tri-acylated lipopeptide. *Cell.* 2007;130:1071–1082. https://doi.org/10.1016/j.cell.2007.09.008
25. Lu BL, Williams GM, Brimble MA. TLR2 agonists and their structure-activity relationships. *Org Biomol Chem.* 2020;18:5073–5094. https://doi.org/10.1039/d0ob00942c
26. Fletcher LD, et al. Vaccine potential of the Neisseria meningitidis 2086 lipoprotein. *Infect Immun.* 2004;72:2088–2100. https://doi.org/10.1128/IAI.72.4.2088-2100.2004
27. Liu B, et al. A vaccine based on the receptor-binding domain of the spike protein expressed in glycoengineered pichia pastoris targeting SARS-CoV-2 stimulates neutralizing and protective antibody responses. *Engineering.* 2022;13:107–115. https://doi.org/10.1016/j.eng.2021.06.012
28. Hantke K, Braun V. Covalent binding of lipid to protein. Diglyceride and amide-linked fatty acid at the N-terminal end of the murein-lipoprotein of the Escherichia coli outer membrane. *Eur J Biochem.* 1973;34:284–296. https://doi.org/10.1111/j.1432-1033.1973.tb02757.x
29. Sung JW, et al. Biochemical characterizations of Escherichia coli-expressed protective antigen Ag473 of Neisseria meningitides group B. *Vaccine.* 2010;28:8175–8182. https://doi.org/10.1016/j.vaccine.2010.09.091
30. Green BA, Farley JE, Quinn-Dey T, Deich RA, Zlotnick GW. The e (P4) outer membrane protein of Haemophilus influenzae: biologic activity of anti-e serum and cloning and sequencing of the structural gene. *Infect Immun.* 1991;59:3191–3198. https://doi.org/10.1128/iai.59.9.3191-3198.1991
31. Zom GG, et al. Novel TLR2-binding adjuvant induces enhanced T cell responses and tumor eradication. *J Immunother Cancer.* 2018;6:146. https://doi.org/10.1186/s40425-018-0455-2
32. Liu B, et al. Recombinant H7 hemagglutinin expressed in glycoengineered Pichia pastoris forms nanoparticles that protect mice from challenge with H7N9 influenza virus. *Vaccine.* 2020;38:7938–7948. https://doi.org/10.1016/j.vaccine.2020.10.061
33. Xu H, et al. A bivalent subunit vaccine efficiently produced in Pichia pastoris against SARS-CoV-2 and emerging variants. *Front Microbiol.* 2022;13:1093080. https://doi.org/10.3389/fmicb.2022.1093080
34. Wang T, et al. A delta-omicron bivalent subunit vaccine elicited antibody responses in mice against both ancestral and variant strains of SARS-CoV-2. *Vaccines.* 2023;11. https://doi.org/10.3390/vaccines11101539
35. Marchesini Tovar G, Gallen C, Bergsbaken T. CD8+ tissue-resident memory T cells: versatile guardians of the tissue. *J Immunol.* 2024;212:361–368. https://doi.org/10.4049/jimmunol.2300399
36. Luangrath MA, Schmidt ME, Hartwig SM, Varga SM. Tissue-resident memory T cells in the lungs protect against acute respiratory syncytial virus infection. *Immunohorizons.* 2021;5:59–69. https://doi.org/10.4049/immunohorizons.2000067
37. Li P, et al. Role of glycosylation mutations at the N-terminal domain of SARS-CoV-2 XEC variant in immune evasion, cell-cell fusion, and spike stability. *J Virol.* 2025;99:e0024225. https://doi.org/10.1128/jvi.00242-25
38. Harrison AG, Lin T, Wang P. Mechanisms of SARS-CoV-2 transmission and pathogenesis. *Trends Immunol.* 2020;41:1100–1115. https://doi.org/10.1016/j.it.2020.10.004
39. Kiyono H, Ernst PB. Nasal vaccines for respiratory infections. *Nature.* 2025;641:321–330. https://doi.org/10.1038/s41586-025-08910-6
40. Excler JL, Saville M, Berkley S, Kim JH. Vaccine development for emerging infectious diseases. *Nat Med.* 2021;27:591–600. https://doi.org/10.1038/s41591-021-01301-0
41. Watanabe Y, Allen JD, Wrapp D, McLellan JS, Crispin M. Site-specific glycan analysis of the SARS-CoV-2 spike. *Science.* 2020;369:330–333. https://doi.org/10.1126/science.abb9983
42. Chen HW, et al. A novel technology for the production of a heterologous lipoprotein immunogen in high yield has implications for the field of vaccine design. *Vaccine.* 2009;27:1400–1409. https://doi.org/10.1016/j.vaccine.2008.12.043
43. Zhu D, Barniak V, Zhang Y, Green B, Zlotnick G. Intranasal immunization of mice with recombinant lipidated P2086 protein reduces nasal colonization of group B Neisseria meningitidis. *Vaccine.* 2006;24:5420–5425. https://doi.org/10.1016/j.vaccine.2006.03.051
44. Hunter CA, Jones SA. IL-6 as a keystone cytokine in health and disease. *Nat Immunol.* 2015;16:448–457. https://doi.org/10.1038/ni.3153
45. Mohd Zawawi Z, et al. Prospective roles of tumor necrosis factor-alpha (TNF-α) in COVID-19: prognosis, therapeutic and management. *Int J Mol Sci.* 2023;24. https://doi.org/10.3390/ijms24076142
46. Song YC, et al. A purified recombinant lipopeptide as adjuvant for cancer immunotherapy. *Biomed Res Int.* 2014;2014:349783. https://doi.org/10.1155/2014/349783
47. Wu S, et al. A single dose of an adenovirus-vectored vaccine provides protection against SARS-CoV-2 challenge. *Nat Commun.* 2020;11:4081. https://doi.org/10.1038/s41467-020-17972-1
48. Sakurai F, Tachibana M, Mizuguchi H. Adenovirus vector-based vaccine for infectious diseases. *Drug Metab Pharm.* 2022;42:100432. https://doi.org/10.1016/j.dmpk.2021.100432
49. Schmidt KG, et al. Detection of pre-existing neutralizing antibodies against Ad26 in HIV-1-infected individuals not responding to the Ad26.COV2.S vaccine. *Infection.* 2023;51:1657–1667. https://doi.org/10.1007/s15010-023-02035-6
50. Teng Z, et al. Bridging nanoplatform and vaccine delivery, a landscape of strategy to enhance nasal immunity. *J Control Release.* 2022;351:456–475. https://doi.org/10.1016/j.jconrel.2022.09.044
51. Marks KE, et al. Toll-like receptor 2 induces pathogenicity in Th17 cells and reveals a role for IPCEF in regulating Th17 cell migration. *Cell Rep.* 2021;35:109303. https://doi.org/10.1016/j.celrep.2021.109303